Title

Automatic airway wall segmentation and thickness measurement for long-range optical coherence tomography images

ISBN

9781628419313

Authors

Qi, Li

Huang, Shenghai

Heidari, Andrew E

et al.

Publication Date

2016-03-08

DOI

10.1117/12.2214605

Automatic airway wall segmentation and thickness measurement for long-range optical coherence tomography images

Li Qi[a,c], Shenghai Huang[a], Andrew E. Heidari[a], Cuixia Dai[a], Jiang Zhu[a], Xuping Zhang[c], Zhongping Chen*[a,b]

[a]Beckman Laser Institute, University of California, Irvine, Irvine, CA, USA 92612; [b]Department of Biomedical Engineering, University of California, Irvine, Irvine, California 92697, USA; [c]Institute of Optical Communication Engineering, College of Engineering and Applied Science, Nanjing University, Nanjing, Jiangsu, China 210093

ABSTRACT

We present an automatic segmentation method for delineation and quantitative thickness measurement of multiple layers in endoscopic airway optical coherence tomography (OCT) images. The boundaries of the mucosa and the sub-mucosa layers were extracted using a graph-theory-based dynamic programming algorithm. The algorithm was tested with pig airway OCT images acquired with a custom built long range endoscopic OCT system. The performance of the algorithm was demonstrated by cross-validation between auto and manual segmentation experiments. Quantitative thicknesses changes in the mucosal layers are obtained automatically for smoke inhalation injury experiments.

Keywords: Optical Coherence Tomography, endoscopic imaging, image processing

1. INTRODUCTION

Imaging the sub-surface structure of the airway wall is of great significance to detect abnormalities during airway injuries. Smoke exposure and inhalation risks, including thermal, toxic, and chemical injuries, result in airway hyperemia, edema, sloughing and necrosis [1, 2]. Pathophysiological information of the injured airway wall, such as the thickness of the mucosal, the gathering of mucosal layer, and the deformation of the airway lumen, could provide better diagnosis of respiratory decreases [3-5]. As a nonionizing, non-invasive medical imaging modality, optical coherence tomography (OCT) has been used to perform high resolution, cross-sectional imaging of biological tissues. Previous studies [6-11] such as the Fourier domain long-range swept source OCT (LR-SSOCT) have demonstrated the flexibility to image the airways of different animals in vivo. Figure 1 shows the OCT images of one cross-section in a sheep airway acquired by our recently reported improved LR-SSOCT system [10, 11]. As shown in Fig. 1 (d), the enlarged detail clearly depicts multiple structures of the airway wall, which include the cartilage, the mucosa, the submucosa, and the mucus.

The identification of different structures in the OCT images is of great importance for quantitative evaluation of airway injury. However, although we have already obtained high resolution airway wall OCT images, the classification of the airway wall structures are mainly based on manual labeling of the boundaries [13], which is time-consuming and subjected to inter-observer errors. A clustering algorithm is used to segment the airway structure from the background [14], but the airway layers are not detected. A morphological and thresholding method is used to identify these layers [15]; however, the method is not robust enough to handle speckle noise and missing features in quality degraded images. No other method has been reported on the auto-segmentation of airway wall structures on OCT images other than this method

In order to robustly segment different airway wall structures and provide quantitative information of these structures automatically, we present a graph-theory-based segmentation algorithm using Cartesian airway OCT images as input. The quantification of the average layer thicknesses can be obtained after the precise localization of different layer boundaries. This algorithm was tested with pig airway images acquired by our LR-SSOCT system [11]. The results show that our algorithm can achieve accurate, robust, and fully automatic delineation of multiple structures in airway OCT images.

Optical Coherence Tomography and Coherence Domain Optical Methods in Biomedicine XX, edited by Joseph A. Izatt, James G. Fujimoto, Valery V. Tuchin, Proc. of SPIE Vol. 9697, 96973B · © 2016 SPIE · CCC code: 1605-7422/16/$18 · doi: 10.1117/12.2214605

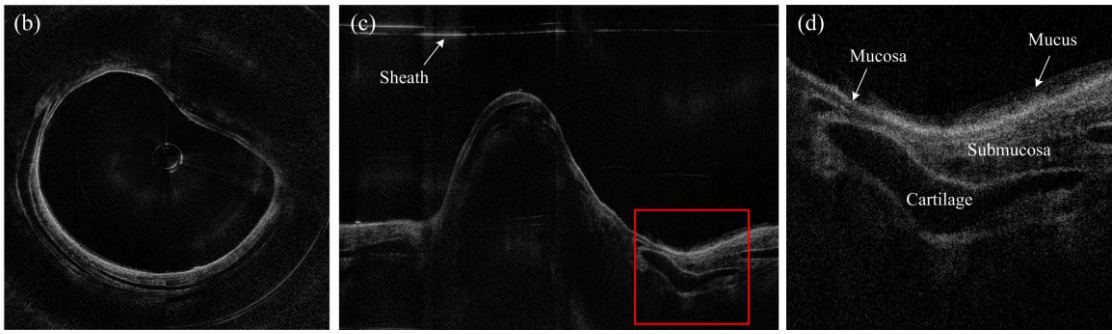

Figure 1. Sample image acquired by the long range SS-OCT system: (a) circumferential image, (b) Cartesian image, and (c) enlarged airway regions in (b).

2. METHOD

As shown in Fig. 2, the proposed algorithm works in three steps: 1) the pre-processing step, which localizes the potential airway wall regions by using a number of denoising and morphological operations； 2) the edge delineation step, which detects the exact locations of the airway lumen, the mucosa/submucosa boundary, and the submucosa/cartilage boundary using the dynamic programming algorithm; and 3) layer thicknesses measurement step, where the average thickness of two mucosal layers are calculated.

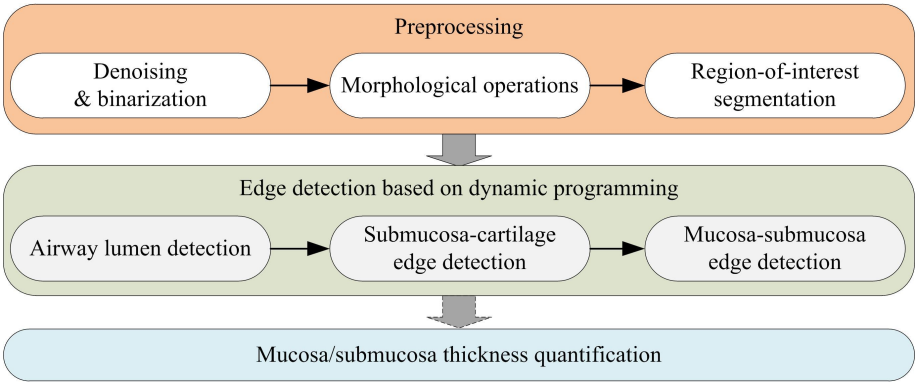

Figure 2. The workflow of the proposed automatic detection algorithm.

The OCT images are generally distorted by multiple defects, such as the speckle noise, the mirror image/objects induced by the Fourier transformation, and the ghost objects produced by internal interference of the optics. To filter out these obstructions, the pre-processing step performs the following operations. After median filtering, the image is transformed to a black and white image by a pre-defined intensity threshold. Then the connected BW regions that could be potentially considered as the airway structure are picked out given two criteria: minimum area and maximum number of regions. In this way, the major component in the image (the airway structure) could be identified from the background.

In the second step, we used the dynamic programming (DP) algorithm [16] to localize the precise edge position. The major feature of the DP algorithm, when applied to edge detection, is that it can preserve the continuity of the boundary, which means that it is less affected by outliers. Using this algorithm, each pixel in the image is considered a node in a graph and thus the edge detection process is transformed to a shortest-path finding problem. For each edge, a single graph is first constructed from the gradient of the original OCT image after flattening using a previously delineated airway region; then the solution of the graph is found recursively by finding the optimal path that has a minimum total cost. The final edge is refined by averaging neighboring edge pixels. Figure 3 shows the intermediate and the final results of the proposed algorithm on a sample image. Finally, after the delineation of the whole airway structure, only the regions that are penetrated by the OCT beam with an orthogonal direction are selected to quantify the airway layer thickness.

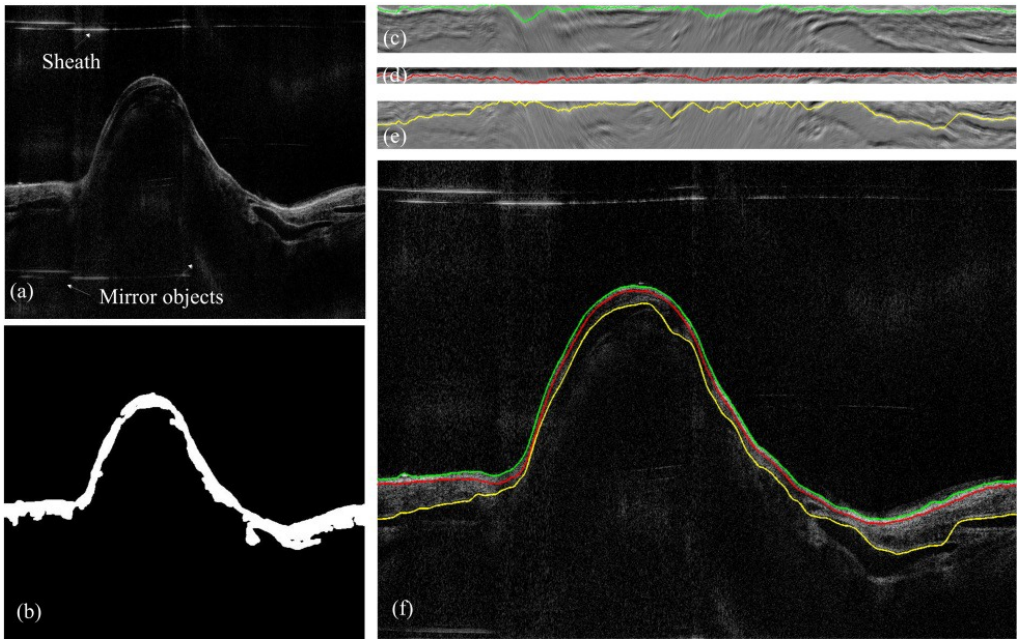

Figure 3. (a) The original OCT image; (b) the segmented airway structure after pre-processing; (c), (d) and (e) the graph constructed from the gradient images of the airway lumen, the mucosa and the submucosa layers, respectively; the color lines depict the localized shortest path; (f) the final edge detection result.

3. RESULTS

3.1 OCT system setup and animal preparation

To verify the flexibility of our algorithm, the images acquired by the LR-SSOCT system reported by our group previously [10, 11] were used as the test set. The LR-SSOCT system utilizes a customized imaging probe that rotates at 1500 rpm with a pullback speed of 12.5mm/s. In order to achieve long range imaging, the probe is designed to have an extended working distance of 20 mm, and the axial resolution is 10 μm in tissue. Imaging of airways with a maximum diameter of 50 mm and 20 cm length can be achieved with this system.

Specifically, OCT image data sets of a pig airway acquired by this LR-SSOCT system were used. These images were taken on a convenience sample from an ongoing study which involves a clinically relevant model of lung failure due to inhalation of wood bark smoke and cutaneous burn. Uninjured baseline airway OCT images were acquired after induction of anesthesia to the animals. Additionally, for monitoring the conditions and progression of smoke inhalation injury, OCT images were acquired after smoke inhalation injury was induced [17].

3.2 Auto-manual segmentation comparison

To verify the flexibility of our algorithm, cross validation between auto- and manual-segmentation was performed on the OCT airway images acquired in pig upper airway with a maximum diameter of 30mm. Specifically, the manual segmentation was done by clicking 30-50 points on an edge and then spline-fitting these points to determine the actual edge. The spline-fitting curve could be modified by adding or removing specific control points until the annotator was satisfied with the result. In a total of 50 frames (image size: 2000×2000 pixels) of the healthy pig airway OCT images picked randomly from a dataset of 200 images were manually annotated. Among the results, all three edges of interest were detected. Figure 4 illustrates the edge detection results in different frames in baseline data sets of the pig samples. As can be seen, even when some of the airway wall was not in the OCT imaging zone with the highest sensitivity, the airway wall was detected accurately. Also, the algorithm could effectively deal with the bifurcation of the airway; the layers in the disconnected areas were extracted successfully.

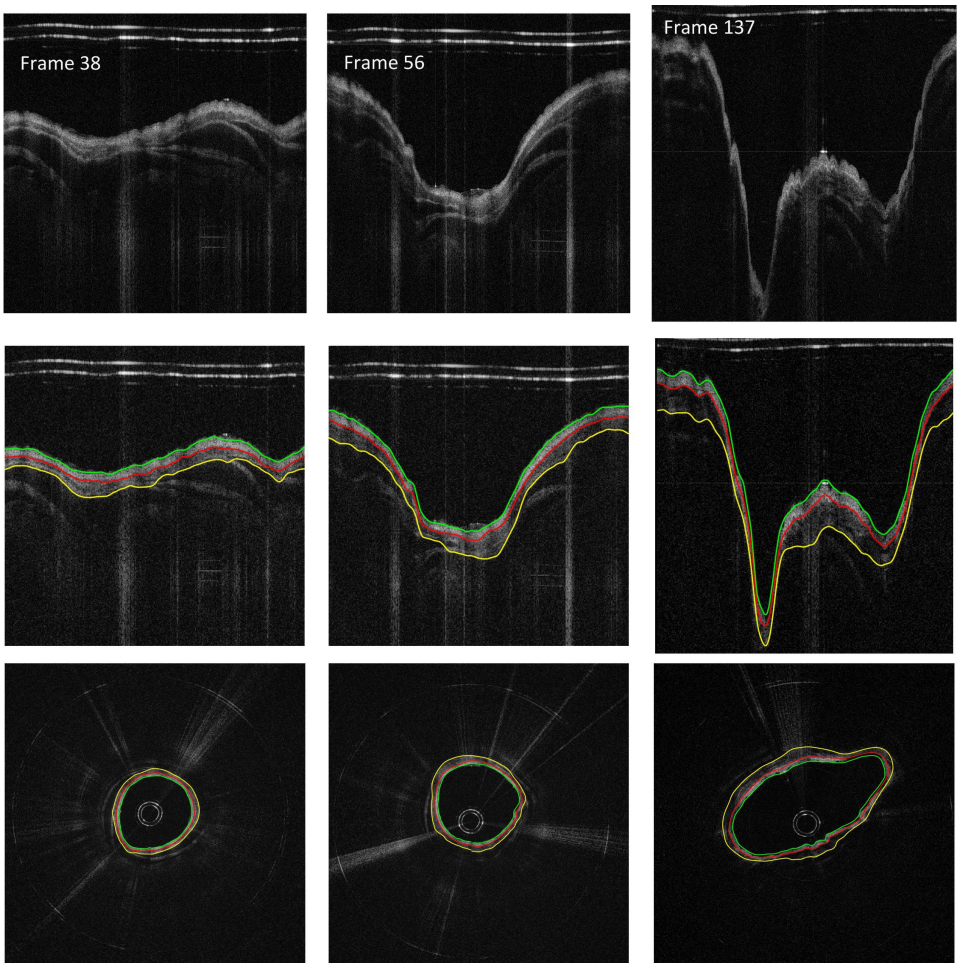

Figure 4. Illustration of the edge detection results in different OCT airway images taken from the pig data set. From top down: the original images, the Cartesian coordinate images with edge detected, the circumferential images.

To quantify the measurement accuracy of the proposed segmentation algorithm against manual segmentation, two validation metrics are used: the root mean square error (RMSE) and the mean absolute deviation (MAD), which are given by:

$$RMSE = \sqrt{\frac{1}{n}\sum_{i=1}^{n}(A_i - M_i)^2}$$
$$MAD = \frac{1}{n}\sum_{i=1}^{n}|A_i - M_i| \quad (1)$$

where A is the auto-segmentation result, M is the manual-segmentation result, and n is the total number of pixels. We compared the auto-manual segmentation accuracy in the airway regions with clear layer structures, and the results are listed in Table.1. Compared to the penetration depth of the LR-SSOCT system, which is about 2mm, the deviation of the auto and manual segmentation results is less than 1% of the total tissue depth. The localization of the airway lumen and the mucosa/submucosa edge are more accurate than that of the submucosa/cartilage edge; this is believed to be caused by the signal degradation in deeper tissue.

Table 1. Comparison of manual and automatic segmentation results.

Item	RMSE	MAD		
	Pixels	Microns	Pixels	Microns
Airway wall lumen	0.8789	10.5462	0.7781	10.8117
Mucosa/submucosa edge	1.9323	23.1876	1.1823	14.1876
Submucosa/cartilage edge	2.1231	25.4770	1.5482	18.5777

3.3 Airway thickness changes during smoke inhalation measured by the proposed algorithm

The diagnosis of inhalation injury is a primary, unresolved problem in modern burn care. Using the purposed segmentation algorithm, comparable quantitative measurements of the airway layers postinjury could be obtained automatically. For the pig data set, the OCT images acquired at baseline and 1-hr post smoke injury were analyzed using our algorithm. For each time point, 10 images were used for layer thickness measurement. These images were all acquired at the same landmark, which was the right mainstem bronchus near the proximal secondary bronchus branch. As stated previously, only the orthogonally laser penetrating areas of the airway were selected for thickness measurement.

The detection results for the pig airway images in the same location at baseline and post-smoke are shown in Fig. 8. The magnified regions display the automatically selected regions for thickness quantification. The circumferential images (transformed from the Cartesian images below) in the right column of Fig. 5 provide better views of the airway substructures and the segmentation results.

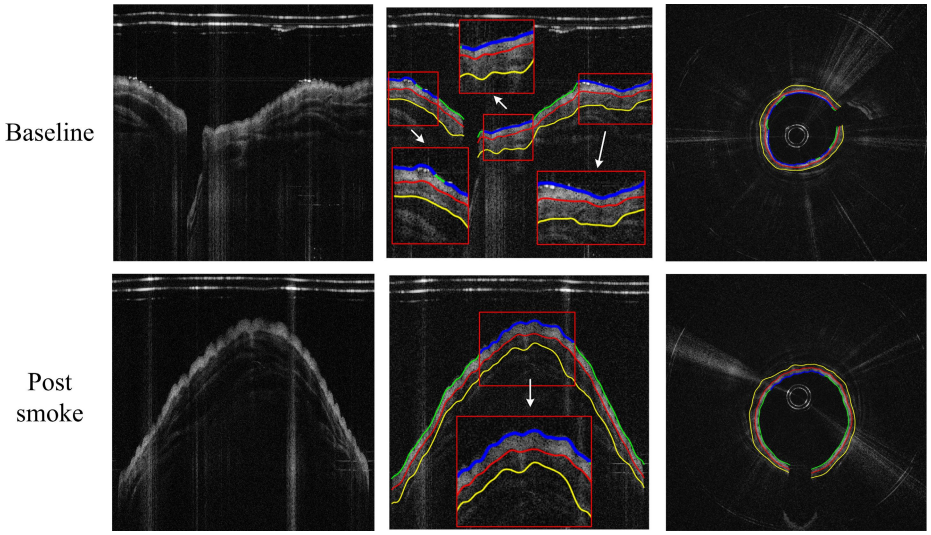

Figure 5. Thickness measurement comparison between baseline and post-smoke images of the pig data set. From left to right: original images, edge extracted images (thickness measured regions enlarged), and circumferential images.

To verify the thickness measured by the automatic algorithm, manual results were obtained on all the images with the same protocol described in Section 3.2. Here, we use three quality metrics for comparison, including Average Thickness (AVGT), Root-Mean-Square Thickness Difference (RMSTD), and Dice's similarity Coefficient (DSC):

$$AVGT = \frac{1}{n}\sum_{i=1}^{n}(A_i^t - A_i^b)$$
$$RMSTD = \sqrt{\frac{1}{n}\sum_{i=1}^{n}[(A_i^t - A_i^b) - (M_i^t - M_i^b)]^2} \quad (2)$$
$$DSC = \frac{2|X \cap Y|}{|X| + |Y|}$$

where A and M are the auto and manual segmentation edges at pixel *i*, with superscript t and b indicating the top and bottom edges, respectively; X and Y are the auto and manual segmented layer regions; and n is the total pixel number.

Table 2 lists the comparison results for the pig data set. Even though the thickness of both the mucosa and submucosa layer increased post smoke, the RMSTD between auto-manual segmentation remained at a relatively low value. The segmentation accuracy for the submucosa layer suffered from a small decrease at the post-smoke time point, and the DSC for the auto-selected region dropped 9.6% compared to the baseline value.

Table 2. Average thickness measurement results for the pig data set*

		auto AVGT		manual AVGT		mean RMSTD		mean DSC
		pixels	mm	pixels	mm	pixels	mm	
Baseline	Layer 1	31.63	0.380	30.55	0.367	2.89	0.035	0.950
	Layer 2	49.44	0.593	48.26	0.579	4.30	0.052	0.953
Post-smoke	Layer 1	40.22	0.483	41.04	0.492	3.68	0.044	0.922
	Layer 2	62.85	0.754	65.20	0.782	8.28	0.099	0.871

*Layer 1: mucosa layer; Layer 2: submucosa layer

4. CONCLUSION

In summary, a fully automatic airway wall structure segmentation method for endoscopic optical coherence tomography images is presented in this paper. The boundaries of the mucosa and the sub-mucosa layers were accurately extracted using a graph-theory-based dynamic programming algorithm. The algorithm was tested with pig airway OCT images. Quantitative thicknesses of the mucosal layers were obtained automatically for the smoke inhalation injury experiments.

REFERENCES

[1] Traber, D. L., Linares, H. A., Herndon, D. N., and Prien, T., "The pathophysiology of inhalation injury--a review," Burns 14(5), 357–364 (1988).

[2] Cox, R. A., Burke, A. S., Soejima, K., Murakami, K., Katahira, J., Traber, L. D., Herndon, D. N., Schmalstieg, F. C., Traber, D. L., and Hawkins, H. K., "Airway obstruction in sheep with burn and smoke inhalation injuries," Am. J. Respir. Cell Mol. Biol. 29(3), 295–302 (2003).

[3] Cancio, L. C., "Current concepts in the pathophysiology and treatment of inhalation injury," J. Trauma 7(1), 19–35 (2005).

[4] Hubbard, G. B., Langlinais, P. C., Shimazu, T., Okerberg, C. V., Mason, A. D., Pruitt, B. A., "The morphology of smoke inhalation injury in sheep," J. Trauma 31(11), 1477–1486 (1991).

[5] Pruitt, B. A., Jr. and Cioffi, W. G., "Diagnosis and treatment of smoke inhalation," J. Intensive Care Med. 10(3), 117–127 (1995).

[6] Ridgway, J. M., Ahuja, G., Guo, S., Su, J., Mahmood, U., Chen, Z., and Wong, B., "Imaging of the pediatric airway using optical coherence tomography," Laryngoscope 117(12), 2206–2212 (2007).
[7] Brenner, M., Kreuter K., Ju, J., Mahon, S., Tseng, L., Mukai, D., Burney, T., Guo, S., Su, J., Tran, A., Batchinsky, A., Cancio, L. C., Narula, N., and Chen, Z., "In vivo optical coherence tomography detection of differences in regional large airway smoke inhalation induced injury in a rabbit model," J. Biomed. Opt. 13(3), 034001-034001-8 (2008).
[8] Yin, J., Liu, G., Zhang, J., Yu, L., Mahon, S., Mukai, D., Brenner, M., and Chen, Z., "In vivo early detection of smoke-induced airway injury using three-dimensional swept-source optical coherence tomography," J. Biomed. Opt. 14(6), 060503-060503-3 (2009).
[9] Lee, S.-W., Heidary, A. E., Yoon, D., Mukai, D., Ramalingam, T., Mahon, S., Yin, J., Jing, J., Liu, G., Chen, Z., and M. Brenner, "Quantification of airway thickness changes in smoke-inhalation injury using in-vivo 3-D endoscopic frequency-domain optical coherence tomography," Biomed. Opt. Express 2(2), 243–254 (2011).
[10] Jing, J., Zhang, J., Loy, A. C., Wong, B. J. F., and Chen, Z., "High-speed upper-airway imaging using full-range optical coherence tomography," J. Biomed. Opt. 17(11), 110507-110507-3 (2012).
[11] Chou, L., Batchinsky, A., Belenkiy, S., Jing, J., Ramalingam, T., Brenner, M., and Chen, Z., "In vivo detection of inhalation injury in large airway using three-dimensional long-range swept-source optical coherence tomography," J. Biomed. Opt. 19(3), 36018-36018-6 (2014).
[12] Zhang, J., Nelson, J. S., and Chen, Z., "Removal of a mirror image and enhancement of the signal-to-noise ratio in Fourier-domain optical coherence tomography using an electro-optic phase modulator," Opt. Lett. 30, 147-149 (2005).
[13] Lee, A. M. Kirby, D., M., Ohtani, K., Candido, T., Shalansky, R., MacAulay, C., English, J., Finley, R., Lam, S., Coxson, H. O., and Lane, P., "Validation of Airway Wall Measurements by Optical Coherence Tomography in Porcine Airways," PLoS One 9(6), e100145 (2014).
[14] Heydarian, M., Choy, S., Wheatley, A., McCormack, D., Coxson, H. O., Lam, S., and Parraga, G., "Automated segmentation of lung airway wall area measurements from bronchoscopic Optical Coherence Tomography imaging," Proc. SPIE 7965(519), 1–9 (2011).
[15] Kirby, M., Lee, A. M. D., Candido, T., Macaulay, C., Lane, P., Lam, S., and Coxson, H. O., "Automated Segmentation of Porcine Airway Wall Layers using Optical Coherence Tomography: Comparison with Manual Segmentation and Histology," Proc. SPIE 8927, 1–9 (2014).
[16] Bellman, R., "On the theory of dynamic programming," Proc. Natl. Acad. Sci. U.S.A. 38(8), 716-719 (1952).
[17] Batchinsky, I., Burkett, E., Zanders, Thomas, B.; Chung, K., Regn, D., Jordan, S., Necsoiu, C., Nguyen, R., Hanson, A., and Morris, J., "Comparison of airway pressure release ventilation to conventional mechanical ventilation in the early management of smoke inhalation injury in swine," Crit. Care Med. 39(10), 2314–2321 (2011).